Journal of Marine Research
September 2008; Volume 66 (5) : Pages 589-616
http://dx.doi.org/10.1357/002224008787536790

Cross-shelf structure of coastal upwelling : a two - dimensional extension of Ekman's theory and a mechanism for inner shelf upwelling shut down

Estrade Philippe[1, *], Marchesiello Patrick[2], De Verdière Alain Colin[3], Roy Claude[4, *]

[1] School of Mathematics and Statistics, University of New South Wales, Sydney, Australia
[2] Institut de Recherche pour le Développement, Nouméa, Nouvelle Calédonie
[3] Ifremer, Laboratoire de Physique des Océans, Brest, France
[4] Institut de Recherche pour le Développement, Brest, France

*: Corresponding author : Estrade P., email address : estrade@maths.unsw.edu.au ; Roy C., email address : Claude.Roy@ifremer.fr

Abstract:

Sea-surface temperature images of the coastal upwelling regions off Northwest Africa show that the core of upwelling is sometimes located far from the coast. This has been documented in three regions that share a common feature, namely a wide and shallow continental shelf. This upwelling feature plays a key role in the ecology of the Canary Current System. It creates an innerfront which provides retention for biological material, e.g. fish eggs and larvae, in the highly productive nearshore environment.

An analytical model has been developed based on a two dimensional extension of Ekman's solution. The linear and steady response of a homogeneous ocean forced by an upwelling-favorable wind provides a mechanism for the upwelling separation from the coast. The merging of the surface and bottom Ekman layers induces a very weak cross-shore circulation and a "kinematic barrier" for the Ekman transport divergence. In the case of an alongshore wind, the barrier is located near the isobath $h \approx 0.4D$, where D is the thickness of Ekman layers. This yields an upwelling cell which is essentially concentrated in the region $0.5D < h < 1.25D$, with upwelling occurring preferentially near the isobath $h \approx 0.6D$. It turns out that the cross-shore width of upwelling scales with D/S, the ratio of Ekman depth to bottom topographic slope. The application of this solution to real bathymetric profiles rationalizes, not only the offshore upwelling observations in Northwest Africa, but also the influence of topography on the cross-shelf structure of a wind-driven coastal upwelling. The model also quantifies the effect of the cross-shore wind component showing how it drives the nearshore pressure gradient adjustment and how it affects the upwelling. A linear numerical experiment reproduces the theoretical steady solution, thereby allowing investigation of the transient regime. Relaxation of the hypothesis in the numerical model validates the linear assumption of the theory and then allows investigation of the sensitivity to friction parameterizations and the influence of stratification. The latter leads to an "oscillation" of the upwelling cell with seaward migration driven by outcropping and homogeneization of the water column, and, coastal incursion driven by a "boundary layers splitting" process caused by shoreward advection of the isopycnal dome and stratification of the inner shelf.

1 Introduction

Ekman's 1905 result, that wind forced oceanic mass transport occurs to the right of the wind (in the northern hemisphere) in a shallow layer of fluid, is the cornerstone of upwelling theories. In the vicinity of eastern boundaries, equatorward winds induce a divergence of the offshore directed mass transport, which causes upwelling of deep, cold and nutrient-rich waters. Chemical properties of these waters indicate an origin not deeper than 200 - 300 m (Pond and Pickard 1986). The strength of the Ekman result lies in the fact that it is independent of the viscosity coefficient when the fluid depth is greater than the depth of the upper Ekman layer.

Although upwelling occurs in this region of Ekman transport divergence, it is difficult to assess the offshore limit of this divergence. The three dimensional reality often blurs the picture provided by the essentially two dimensional Ekman theory. Measurements of this divergence are notoriously difficult as the associated vertical velocities are too small to be detected with the present generation of instruments. A two layer model is often used to estimate the order of magnitude of the cross shore scale of coastal upwelling [see (Csanady 1982) for a review]. For an ocean with a flat, deep bottom, it is found that the interface shoals toward the coast with the scale of the internal Rossby radius $R' = \frac{\sqrt{g'h_0}}{f}$ (with g' the reduced gravity and h_0 the small upper layer thickness). This stratification dependent scale varies between 5 and 30 km, and has frequently been used to determine the order of magnitude of vertical velocities associated with coastal upwelling (Hill *et al.* 1998; Pickett and Paduan 2003). Dividing the Ekman volume transport by R' gives a vertical velocity scale $w = O(\frac{\tau}{\rho_0 f R'})$ where τ is the wind stress parallel to the coast. For $f = 10^{-4}\ s^{-1}$, $R' = 20\ km$ and $\tau = 0.1\ Pa$, the estimated vertical velocity is $5\ 10^{-5}\ m.s^{-1}$ ($\approx 4.3\ m.day^{-1}$). This indicates the weakness of estimated vertical circulation which cannot exceed more than a few tens of meters a day. It is therefore "secondary" to coastal geostrophic jets whose speeds are of the order of tens of km a day (or 3 orders of magnitude larger). However, the results of the present study suggest that R' may not be the right scale to estimate the cross shore width of an upwelling cell for shallow topographies.

Numerical models are well adapted tools to study the vertical structure of upwelling if one

is ready to use high resolution in the vicinity of the coast. This has been addressed by Allen et al (1995) and Marchesiello et al (2000) for the narrow shelves of Oregon and New South Wales respectively, Austin and Lentz (2002) for a shallow channel. All these studies use a two dimensional high resolution model, with the latter showing a clear separation of the upwelling cell from the coast. *The central objective of the present study is to understand the causes of this separation.* Several authors in the 1970s and 1980s have studied the possibility of a secondary upwelling over the outer shelf (Hill and Johnson 1974; Tomczak and Käse 1974; Johnson and Killworth 1975; Hsueh and Ou 1975; Johnson and Manja 1979; Lill 1979; Johnson and Nurser 1983); they proposed interesting mechanisms inducing a *secondary* cell, but did not address the problem of the *main* upwelling cell separating from the coast, which requires consideration of the inner shelf. In this study, a cross shore extension of the classical 1905 Ekman's solution is derived and this new two dimensional solution clarifies the basic mechanism of upwelling separation from the coast : Upwelling occurs offshore from a "kinematic barrier" to the cross shelf flow, which results from the complete merging of the upper and lower Ekman layers in shallow depths.

Most observations of Sea Surface Temperature (SST) in upwelling coastal regions show a minimum at the coast, bearing witness to the existence of cold water upwelling. Some indications on upwelling intensities can be obtained from the SST signal, but the geographical distribution of vertical velocities remains elusive due to the spreading and mixing of upwelled water with the surrounding water. Often the coldest water is stirred into long filaments far from the coast, a process usually observed downstream of capes. In such cases, the vertical circulation occurs near the coast forming a temperature front, which becomes unstable and generates mesoscale eddies (Brink 1983b). However in the three main regions of the Canary System where the continental shelf is wide and shallow (figure 1a), both SST observations and in situ data show more stable structures with the SST minimum located away from the coast (figure 1b). These atypical structures are shaped as cold tongues surrounded by warmer water masses both on the offshore *and* inshore side of the tongues. They have been observed during upwelling events off Southern Morocco (Barton *et al.* 1977), and on longer seasonal time scales both in the Arguin Bank region (Demarcq and Faure 2000) and off

South Senegal (Roy 1998). These structures are not generated by mesoscale activities, but are the signature of upwelling occurring at a very large distance from the coast (as far as 100 km off Southern Morocco).

Such configurations of coastal upwelling have an impact on the ecology. In upwelling systems, fish tend to avoid spawning in areas characterized by strong offshore transport and wind mixing. Spawning grounds are usually located outside of the main upwelling centres and spawning seasons are tuned to avoid the peak of upwelling season (Parrish *et al.* 1983). Figure 1 shows the close relationship between shelf geometry, upwelling response, and dynamics of fish spawning in the Canary Current System. Two different strategies can be identified in figure 1c. North of 25^oN, spawning follows the usual scheme, with the major spawning period being out of phase with the upwelling season. South of 25^oN, an unusual pattern is recorded with fish spawning grounds being located *within* major upwelling regions and spawning occurring *during* the upwelling season. This unusual spawning pattern has been related to enhanced retention of fish eggs and larvae within the highly productive coastal environment (Roy *et al.* 1989; Roy 1998). Enhanced retention is suggested to result from the presence of a nearshore kinematic barrier that prevents biological materials being transported in the open ocean domain. In the northern region, the absence of broad shelves prevents upwelling separation from the coast, thereby preventing a suitable combination of upwelling and retention processes considered to be major drivers of fish reproductive strategy (Bakun 1996).

If the consequences on the biology of "upwelling separation from the coast" phenomenon is documented, the physical processes which lead to this separation remain to be identified. Topography, wind variability, and stratification are among the main environmental factors to be considered in generating the observed upwelling structure. Shelf geometry seems to be of greatest influence in terms of upwelling separation because the presence of a broad shallow shelf appears as a necessary condition for its observation (along with an upwelling favorable wind, of course). The two other factors also exert an influence on this process : wind stress variability directly influences the upwelling response; stratification limits the thickness of surface and bottom boundary layers and also directly influences the density front intensity delineating the boundaries of upwelled cold water tongues. This paper

concentrates on the first factor, shelf geometry, however wind orientation and stratification influences are briefly adressed. It is essentially shown here how inner shelf geometry influences the cross shore structure of upwelling. First, Welander's (1957) method to extend the one dimensional Ekman's (1905) model to horizontal dimensions is recalled in section 2. Then the analytical solution over any cross shore topography is derived in section 3. The use of ROMS numerical model (Shchepetkin and McWilliams 2005) in section 4, cross validates both models (theoretical and numerical), provides the transient formations of upwelling and allows to explore the solution in a more realistic context by relaxing some hypothesis (addition of : non-linear terms, more sophisticated turbulent closures, stratification). These results are further discussed in section 5.

2 Background (How to extend 1D Ekman's model to horizontal dimensions using Welander's method)

Welander (1957) has derived the methods through which the original Ekman model could be extended over varying bottom topography but has not applied them to specific wind and topography configurations. Yet, it is shown in the next section that the assumption of no long shore variations leads to a particularly simple analytical solution. In the present section the one dimensional Ekman's model is discussed and recalled using Welander's formalism.

Ekman (1905) has found the stationary response to a constant steady wind, assuming that the downward transfer of momentum is carried out by turbulence generated by shear instabilities and parameterized by a constant eddy viscosity. The assumption of a constant eddy viscosity is somewhat difficult to defend, since it is known from the work of Prandtl that the "mixing length" must be reduced as horizontal boundaries are approached. The second assumption of a homogeneous ocean is invalidated by many geophysical contexts. Building a theory which includes bottom friction, varying topography, and stratification is a daunting task which remains to be carried out for the coastal upwelling problem. Csanady (1982) summarizes this in his book on circulation in the coastal ocean, by saying "the main source of complexity in density-driven motions is the coupling of the velocity

and density fields". In response, a number of works have addressed this problem [see (Garrett *et al.* 1993) for a review] and show how the buoyancy force on a slope may considerably alter the Ekman picture by isolating the interior flow from frictional influences at the boundary. However, the homogeneous problem is still relevant for shallow seas, which is the main focus of this paper. Over shallow topography, the fluid is well mixed and stratification is generally weak. In addition, the homogeneous problem is an important first step in order to consider the stratified case. Some of the processes associated with the density stratification which bear upon upwelling separation from the coast are examined in section 4-(iv) with the help of a primitive equation ocean model. Another assumption of Ekman's theory is that eddy-driven lateral fluxes can be neglected. The coastal margin of the ocean is often observed to be an area of active mesoscale turbulence caused by baroclinic and barotropic instability processes which are often parameterized assuming some type of lateral eddy viscosity. Even under the approximation of a constant eddy viscosity, Pedlosky (1987) has noted the difficulty of solving Ekman's model with both lateral friction and varying bottom topography. In Ekman's original problem, the advection terms vanish identically because the forcing is uniform and the coastal boundary and topographic variability are not considered. Therefore, under Ekman's hypothesis, the horizontal momentum equations for a steady motion reduce to :

$$f\underline{k} \wedge \underline{u} = -\frac{\nabla p}{\rho_0} + A_v \frac{\partial^2 \underline{u}}{\partial z^2}$$

where the Coriolis parameter f is assumed uniform given the small horizontal scale compared to the Earth radius ($\underline{k}$ is a vertical unit vector). The pressure p is assumed to be hydrostatic on account of large horizontal scales over vertical ones. Separating the horizontal velocity components into geostrophic and Ekman components, we have :

$$f\underline{k} \wedge \underline{u}_g = -\frac{\nabla p}{\rho_0}$$

where $\underline{u}_g$ is horizontally non divergent. The Ekman components satisfy :

$$f\underline{k} \wedge \underline{u}_e = A_v \frac{\partial^2 \underline{u}_e}{\partial z^2} \tag{1}$$

Since $\underline{u}_g$ is depth independent, the boundary conditions at the surface are :

$$z = 0 \ : \qquad A_v \frac{\partial \underline{u}_e}{\partial z} = \frac{\underline{\tau}_s}{\rho_0} \tag{2}$$

where $\underline{\tau}_s$ is the wind stress (assumed constant). At the lower boundary, bottom friction reduces velocity to zero (no slip condition) :

$$z = -h \ : \qquad \underline{u}_e + \underline{u}_g = 0 \tag{3}$$

The solutions of these equations are conveniently obtained in terms of the complex variables $\tilde{u}_e = u_e + i\, v_e$, $\tilde{u}_g = u_g + i\, v_g$ and $\tilde{\tau}_s = \tau_s^x + i\, \tau_s^y$. Equations (1), (2) and (3) become:

$$\frac{\partial^2 \tilde{u}_e}{\partial z^2} - c^2\, \tilde{u}_e = 0 \tag{4}$$

$$z = 0 \ : \qquad A_v \frac{\partial \tilde{u}_e}{\partial z} = \frac{\tilde{\tau}_s}{\rho_0} \tag{5}$$

$$z = -h \ : \qquad \tilde{u}_e + \tilde{u}_g = 0 \tag{6}$$

where $c = (1+i\gamma)\frac{\pi}{D}$ with $\gamma = \frac{f}{|f|}$ and $D = \pi\sqrt{\frac{2A_v}{|f|}}$ the Ekman depth. The important adimensional parameter governing the solutions of these equations is $\frac{h}{D} = \frac{1}{\pi\sqrt{2}} E_v^{-1/2}$ where $E_v = \frac{A_v}{|f|h^2}$ is the Ekman number. Depending on the value of the local depth, Coriolis forces are expected to be important or unimportant according to a small or large value of the Ekman number. The 1D Ekman's solution is readily obtained by solving (4) with boundary conditions (5) and (6) :

$$\tilde{u}_e = \tilde{u}_0 \frac{\sinh[c(z+h)]}{\cosh[ch]} \ - \ \tilde{u}_g \frac{\cosh[cz]}{\cosh[ch]} \tag{7}$$

where $\tilde{u}_0 = u_0 + i\, v_0 = (1 - i\gamma)\frac{\pi\tilde{\tau}_s}{\rho_0 |f| D}$ is the surface Ekman velocity in the deep ocean limit. In Ekman's original problem, wind stress is constant in space, so that $\underline{u}_e$ is independent of horizontal coordinates and vertical velocities vanish identically. However, with varying bottom topography, this

is not the case anymore. With a rigid lid at the free surface, the continuity equation integrated from top to bottom yields :

$$\nabla_H . \underline{U}_e + \underline{u}_g . \nabla h = 0 \tag{8}$$

where $\underline{U}_e = \int_{-h}^{0} \underline{u}_e \, dz$. Defining $\underline{U}_e^s = \int_{z}^{0} \underline{u}_e \, dz'$ as the Ekman transport integrated from the top to depth z yields the vertical velocity :

$$w = \nabla_H . \underline{U}_e^s \tag{9}$$

Following Welander (1957), we now introduce horizontally varying structure functions which allow to present the solutions in a compact form and ease their physical interpretations (Brink 1983a; Mitchum and Clarke 1986). These structure functions F_i, S_i and T_i are defined and shown in figure 2 as functions of $\eta = \frac{\pi h}{D}$. The Ekman transport is obtained by the integration of (7) over the entire water column :

$$\underline{U}_e = -(1 - S_1)\, \underline{k} \wedge \frac{\underline{\tau}_s}{\rho_0 f} + S_2 \frac{\underline{\tau}_s}{\rho_0 f} \; + \; \frac{D}{2\pi} \Big[\, (\gamma T_1 - T_2)\, \underline{k} \wedge \underline{u}_g \; - \; (T_1 + \gamma T_2)\, \underline{u}_g \, \Big] \tag{10}$$

The cumulative transport from the surface to depth z is :

$$\tilde{U}_e^s = \frac{1}{c} \Big[\, \tilde{u}_0 \, (1 - \frac{\cosh[c(z+h)]}{\cosh[ch]}) \; + \; \tilde{u}_g \, \frac{\sinh[cz]}{\cosh[ch]} \, \Big] \tag{11}$$

Equation (12) is obtained when (10) is inserted into the mass conservation equation (8) :

$$\begin{aligned} \frac{D}{2\pi} \Big\{ \quad & (\gamma T_1 - T_2)\, \nabla^2 p \; + \; \tfrac{\pi}{D} \nabla h \, . \Big[\, (T_1' + \gamma T_2' - 1)\, \underline{k} \wedge \nabla p + (\gamma T_1' - T_2')\, \nabla p \, \Big] \quad \Big\} = \\ & (1 - S_1)\, \mathrm{curl}\, (\underline{\tau}_s) + S_2 \nabla \, . \, \underline{\tau}_s + \tfrac{\pi}{D} \nabla h \, . \Big[\, S_1' \, \underline{k} \wedge \underline{\tau}_s + S_2' \, \underline{\tau}_s \, \Big] \end{aligned} \tag{12}$$

This equation, first derived by Welander (1957, page 48), shows how to compute the pressure field (hence the geostrophic flow) adjusted to wind forcing and topography. In principle, this elliptic equation can be solved numerically in a closed basin, assuming that the transport normal to the coast

vanishes. It is shown in the next section that an analytical solution can be obtained in the absence of long shore variations. Note that the vertical profiles of coastal circulation given by Ekman (1905, page 53) are mass conserving, because for each depth he has computed the geostrophic current imposed by the boundary condition at the coast. However, he did not explore this idea further. Using Welander's formalism, we will next derive the mass conserving cross shore profile of geostrophic velocity, thereby extending Ekman's one dimensional solution to the case of varying cross shore bottom topography.

3 Two dimensional (cross shelf) extension

Let us consider the case of a semi infinite ocean bounded by an eastern meridional coast and assume further that long shore variations in either the forcing fields or the geometry are negligible so that $\frac{\partial}{\partial y}$ derivatives vanish. Therefore, the zonal geostrophic component u_g is zero. As is shown next, the alongshore geostrophic flow can easily be determined because (8) reduces to :

$$\partial_x U_e = 0$$

and the Ekman transport (10) becomes :

$$U_e = (1 - S_1)\,\frac{\tau_s^y}{\rho_0 f} + S_2\,\frac{\tau_s^x}{\rho_0 f} - \frac{D}{2\pi}\,(\gamma T_1 - T_2) v_g$$

The transport U_e which vanishes at the coast, *must therefore vanish everywhere* giving v_g :

$$v_g = \frac{2\pi}{\rho_0 f D}\,[\,\frac{1 - S_1}{\gamma T_1 - T_2}\,\tau_s^y + \frac{S_2}{\gamma T_1 - T_2}\,\tau_s^x\,] \tag{13}$$

(i) Alongshore wind forcing

For simplicity, let us consider first the case of a constant alongshore wind forcing ($\tau_s^x = 0$, $\tau_s^y = cste$). The alongshore geostrophic flow (13) becomes :

$$v_g = 2\,v_0\,\frac{1 - S_1}{\gamma T_1 - T_2} \tag{14}$$

where $v_0 = \frac{\pi \tau_s^y}{\rho_0 |f| D}$ is the meridional surface Ekman velocity in the deep limit (note that $u_0 = \gamma v_0$ in this alongshore wind forcing case). The shape of the structure function $\frac{1-S_1}{\gamma T_1 - T_2}$ is shown in figure 2 for $\gamma = 1$. If expression (14) for v_g is now inserted into (7) the horizontal flow field is entirely determined :

$$u + i\,v = (u_0 + i\,v_0)\,\frac{\sinh[c(z+h)]}{\cosh[ch]} + 2\,i\,v_0\,\frac{1-S_1}{\gamma T_1 - T_2}\,(1 - \frac{\cosh[cz]}{\cosh[ch]}) \tag{15}$$

$$w = -v_0\,\frac{\partial h}{\partial x}\,.\,\Re\Big\{\,\sinh[cz]\,(S_1 - iS_2)\,\Big[\,(S_1 - iS_2)\,(\gamma + i + 2i\frac{1-S_1}{\gamma T_1 - T_2}(F_1 + iF_2)) - (\gamma + i)\,(\frac{1-S_1}{\gamma T_1 - T_2})'\,\Big]\,\Big\} \tag{16}$$

where the symbol $\Re$ stands for real part. The vertical velocity in (16) is obtained from (9), (11) and (14). The illustration of the solution can be completed by the calculation of a stream function in this two dimensional case. With $u = -\psi_z$ and $w = \psi_x$, ψ can be simply obtained from (11) and (14) giving $\psi = \Re\,\{\tilde{U}_e^s\}$. These continuous 2D solutions are shown in figures 3 and 4 with respect to the parameter h/D (in the upwelling favorable case $\tau_s^y < 0$ and $f > 0$). Note that, at the difference of the other fields, the vertical velocity also depends on the topographic slope (not only on the depth h). In these solutions h depends on the cross shore coordinate x, just like the structure functions. But since the topography enters only parametrically, the horizontal flow and the stream function can be reconstructed *for any topographic profiles* in the cross shore vertical plane.

Are additional requirements needed for this solution to be valid ? First, the zero normal velocity at the coast is satisfied when h/D goes to zero there. Second, the bottom boundary condition $w = \underline{u}.\nabla h$ is also satisfied everywhere due to the no slip bottom boundary condition. Hence, all boundary conditions are met showing that the 1D Ekman's model can be extended naturally to a 2D configuration. Although Ekman's solutions in the constant wind case are exact solutions of the non linear problem, this is no longer true for solutions (15) and (16) as non linear terms like $u\frac{\partial u}{\partial x}$ and $u\frac{\partial v}{\partial x}$ are not identically zero. Comparing them respectively to fv and fu, two Rossby numbers appear $\frac{U}{V}\cdot\frac{U}{fL_x}$ and $\frac{V}{fL_x}$ where L_x is the cross shore topographic scale. Therefore, the present solution is only

valid provided that the topography scale is such that $L_x \gg \frac{V}{f}$ (because $\frac{U}{V}$ is less than 1). For $V \approx 0.5$ $m.s^{-1}$ and $f \approx 10^{-4}$ s^{-1}, the topographic scale must be much greater than 5 km. Fortunately this condition is satisfied by most of the NW African shelves.

The structure of the horizontal flow is shown in the $(h/D, z/D)$ space in figure 3. Although the solution appears independent of topographic shape in this representation, it is valid for any topographic shape. The flow is scaled by $|v_0|$ which captures all the dependencies from wind stress intensity, turbulent viscosity and latitude. The normalized cross shore flow is nearly zero for h/D less than 0.4. For this parameter setting, *it is as if the condition of zero normal velocity at the coast moved offshore in waters deep enough for the Coriolis forces to be significant.* Inshore, the dynamics naturally impose a flow parallel to the coast without upwelling. In deeper waters, the Ekman currents (directed offshore at the surface, inshore at the bottom) intensify in a region of h/D between 1.5 and 0.5. This region coincides with the divergence region of surface Ekman transport; hence upwelling is to be found there. For larger h/D values, the cross shore secondary flow is concentrated in the two Ekman layers with little flow in between. The alongshore Ekman flow (figure 3b) is downwind near the surface, upwind near the bottom. These two viscous currents thicken as the depth increases in the region of divergence and then stabilize.

The viscous stress magnitude $\rho_0 A_v |\frac{\partial u}{\partial z}|$ normalized by the wind stress is shown in figure 3c. Strong friction occurs in the near shore region ($h/D < 0.5$) with internal stresses larger than 90% of the wind stress. This is caused by the overlap of the surface and bottom Ekman layers. Note the presence of a sublayer in the bottom boundary layer where the stress is even larger than the wind stress. The region of weak stresses when h/D becomes large delineates the geostrophic region.

The stream function (figure 4a) accurately describes the structure of the upwelling overturning cell : 90% of the Ekman current transport upwells for h/D between 1.25 and 0.5. Therefore, if the slope S is constant, the cross shore width of upwelling is equal to $0.75D/S$. More generally, D/S can be interpreted as a representative cross shore length scale for upwelling (see section 5 for a discussion of the implications regarding upwelling indices).

This simple model provides an essential piece of information : there is a critical isobath h_c such

that for smaller depths, frictional forces dominate, the flow becomes polarized alongshore and the divergence of the Ekman transport (hence upwelling) occurs outside this region. This kinematic barrier is $h_c \approx 0.4D$ for alongshore winds. If this barrier is estimated at $h_c = 20$ m for the three Northwest African regions described previously (where upwelling is found typically near the 30 m isobath), the solution requires an Ekman layer thickness of the order of 50 m, which is in good agreement with inferences from observations (Smith 1981; Lentz 1992). Therefore, this solution provides a simple explanation for upwelling separation from the coast in a realistic parameter regime, to the extent that constant mixing coefficients describe adequately the turbulent mixing. Turbulent boundary layers are, of course, more complex with constant stress layers developing near the wall (Tennekes and Lumley 1987) and the present conclusions will have to be checked against a more refined treatment of the boundary layers.

The present theory predicts that a steep continental shelf will favor a narrow and intense upwelling cell, while a gentle slope will favor a broad and weak upwelling cell. The vertical velocity (normalized by $v_0 \frac{\partial h}{\partial x}$ in figure 4b) has maximum near surface values for $h/D \approx 0.6$. With $D \approx 50$ m, SST minima (due to upwelling) are then expected to occur near the isobath $h = 30$ m. In regions like Southern Morocco where stratification is weak, the upwelling cell properties should be consistent with the results of this homogeneous theory. The influence of stratification on the present results is studied in section 4-(iv).

To summarize the theoretical predictions of this "Ekman model over topography", figure 5 presents the various physical processes at work as a function of depth. The crucial role is played by the interaction of Ekman layers for sufficiently shallow depths. The upwelling cell is found in a transition zone between 2 regimes : a coastal regime completely dominated by friction whereby the flow is parallel to the coast, and a deep ocean regime where the top and bottom Ekman layers are well separated (they still interact but indirectly through the interplay of the interior geostrophic flow). The inshore boundary of the transition zone is defined as the place where the top and bottom Ekman layers overlap. Because it encloses an area where no cross shore flow is permitted, this boundary acts as kinematic barrier for Ekman transport. In this area, the frictional effects due to wind and

bottom stresses compensate and maintain the flow in the alongshore direction throughout the entire water column.

(ii) Application to realistic shelf topography

It is straightforward at this point to show the structure of these theoretical upwelling cells over realistic topography. Looking for well-observed yet different upwelling regions, Southern Morocco (broad and shallow shelf) and Oregon (narrow and deep) are two natural candidates for studying the limits of the model control parameter h/D. The geometric differences of these two bathymetric profiles originate from a geological age difference between young shelves of the Eastern Pacific and older, hence more eroded, shelves of the Eastern Atlantic. GEBCO1 bathymetry is used to construct the profiles. Normalized stream functions are shown in figure 6 for 3 values of D and for any constant southward wind.

Off Morocco the upwelling structure is very sensitive to the Ekman depth (figure 6a) due to shelf shallowness. For $D = 30$ m upwelling occurs over the middle of the shelf at about 25 km to 45 km from the coast. The case $D = 60$ m seems more realistic for Southern Morocco where, as observed by Kundu (1977), the entire water column over the shelf is frictional (with a return flow clearly established in the bottom boundary layer). The solution presents a marked shelf-break upwelling, as well as a weak convergence zone. This two-cell upwelling structure is very consistent with synthesized observations by the SCOR working group (1975) and recalled in figure 7a. The synthesis shows a two-cell structure for Southern Morocco made of a broader, weaker coastal cell and a shelfbreak cell. The analytical model shows that the two-cell structure is caused by the flatness of a 30 km wide midshelf topography (the cross shore scale of upwelling D/S becomes infinite in the flat topography limit). A single, broader and weaker cell is obtained if we use a bathymetric profile off Cape Blanc where the slope rises monotonically (not shown). The theoretical upwelling cell is then closer to the observations synthesized by Mittelstaedt (1983) recalled in figure 7b. In both cases, either two-cell or large one-cell structures are expected to produce the diffuse signal of cold water upwelling generally observed from satellite images of the region. As the Ekman depth

increases ($D = 90$ m), the shelfbreak cell off Morocco becomes stronger at the expense of the coastal cell. This may represent a later stage of upwelling spin up, when the boundary layers have deepened, a situation observed by Barton et al (1977).

Off Oregon, the modelled upwelling cell is trapped near the coast for any values of the Ekman depth (figure 6b). A realistic value of D in this region is 30 m, in which case the model shows a very narrow (2 km), intense upwelling cell. Recent observations by Kirincich et al (2005) have located the upwelling position off a narrow Oregon shelf with relatively good accuracy. These authors show that about 25% of the Ekman transport occurs near the isobath $h = 15$ m within less than 2 km from the coast, and that the bulk is established in 50 m depth within about 5 km from the coast. Ekman divergence therefore occurs on a narrow coastal band. Kirincich et al (2005) succeeded in observing a slight upwelling separation from the coast when stratification weakens near the coast; a process they call "shut down". The Oregon solution for $D = 30$ m (figure 6b) agrees well with these observations. Also in this solution, a thin separation from the coast appears when the Ekman depth increases. However, the present theory does not predict the return onshore flow observed at mid depth off Oregon (the analytical return flow remains in the bottom layer where the friction term can balance the Coriolis term associated with cross shore currents). Kundu (1977) observes that the return flow off Oregon occurs between the ocean floor and the base of the thermocline, where it is intensified. In this case, the interior onshore flow has to be balanced either geostrophically by alongshore pressure gradients (Marchesiello *et al.* 2000), or by non linear cross shelf momentum fluxes (Lentz and Chapman 2004). In the Morocco region, alongshore pressure gradients may be weaker on the shelf because its size affords greater isolation from offshore dynamics and associated mesoscale variability. Clearly, the differences seen in our Oregon and Morocco solutions for cross shelf circulation are very similar to the differences observed and highlighted by the SCOR working group (compare 6a for $D = 60$ m and 6b for $D = 30$ m, with 7a-c).

(iii) Effect of the cross shore wind component

Until now, we have only considered the case of an alongshore wind, but the solutions for any wind orientation can readily be obtained using the method of section 3-(i). When a cross shore component τ_s^x is considered, the insertion of equation (13) into (7) and (11) gives the analytical expression of u, v, w and ψ (not shown).

The cross shore profile of the geostrophic velocity given by (13) is now driven by two structure functions for each wind component. The comparison of these functions in figure 2 shows that the pressure gradient adjustment is controlled by the cross shore component of the wind in shallow water ($h/D < 0.35$), while in deeper water it is still controlled by the alongshore wind component. The resulting geostrophic velocity profile is presented in figure 8 in the cases of an onshore and an offshore wind both upwelling favourable, along with the associated stream function. The onshore wind component drives an opposite sign pressure gradient and a weak downwelling cell in the shallow water near the coast. The offshore wind component amplifies the negative pressure gradient and the upwelling near the coast. As a result the mechanism of upwelling separation from the coast is enhanced by onshore winds and weakened by offshore ones. Besides, the Ekman transport is more (less) concentrated near the surface with an offshore (onshore) wind. This cross shore wind component effect may significantly impact upwelling variability from diurnal (sea breeze) to seasonal scale (for instance continental [maritime] trade winds are prevailing at the begining [end] of the Senegalese upwelling season). Note that the numerical model used in the next section with an alongshore wind, reproduces convincingly the theory for any wind direction as well.

4 Numerical modelling

The primitive equation model ROMS (Shchepetkin and McWilliams 2005) is used next in a cross validation experiment of the analytical results. Furthermore, the numerical model allows us to explore the validity of the hypotheses of the theoretical solution by adding some missing ingredients (namely momentum advection, more sophisticated friction parametrizations and stratification). To obtain a

2D model in the "zonal-depth" plane with ROMS, a north-south periodic channel is constructed with only 3 grid points in the meridional direction. The zonal width of the domain L_x is 200 km with 1 km resolution while the linear topography is $h(x) = 10^{-3}\,(L_x - x) + h_{min}$ with $h_{min} = 4$ m. To resolve the Ekman layers, 60 σ levels are used in the vertical (a refinement of resolution near the surface and bottom is added in the non linear experiment). The variations of the free surface from ROMS are small enough to allow a useful comparison with the rigid lid approximation (free surface anomalies are always much less than h_{min}). At the western offshore end, a radiation boundary condition is used along with a sponge layer of 40 km width with a 10^2 $m^2.s^{-1}$ horizontal viscosity (horizontal harmonic friction vanishes elsewhere). The fluid is homogeneous and at rest at initial time. The forcing is a constant alongshore wind $\tau_s^y = -0.1$ Pa imposed at $t = 0$ over the whole domain. In the cross validation and non linear experiments, the constant vertical viscosity is chosen as $A_v = 4.83\ 10^{-3}$ $m^2.s^{-1}$ corresponding to $D = 50$ m at latitude $15^o N$.

(i) Cross validation experiment

One difference with the previous theory is that the model requires a specific parametrization of the bottom stress instead of the no slip boundary condition. Nevertheless, the no slip condition can be approached using a large drag coefficient value. In the validation experiment, we use a linear bottom friction law $\underline{\tau}_b = -\rho_0\, r\, \underline{u}_b$ with the drag coefficient value $r = 5\ 10^{-3}$ m/s. The sensitivity of the numerical solution to bottom friction parametrization is discussed later in section 4-(iii). Note that the momentum advection is turned off in the validation experiment.

The time evolution of horizontal velocities is shown in figure 9 for several positions across the domain. It allows us to estimate directly the spin up time. In the offshore part ($h/D > 0.5$), the spin up is controlled by damping of the geostrophic flow in the bottom Ekman layer, whereas inshore ($h/D < 0.5$) the spin up occurs through frictional adjustment. The geostrophic component can be clearly observed for $h/D = 1$ and 2.5. For the offshore positions the spin up time is proportional to h/D (*i.e.*, $\propto E_v^{-1/2}$), which is in agreement with the scaling theoretically predicted and observed in laboratory experiments for small E_v [see e.g (Greenspan 1968)]. Since the wind rapidly spins up the

surface layer, the Ekman drift induces a divergence, hence a drop of the free surface and geostrophic flow. The steady state is reached when the geostrophic flow is in equilibrium with the bottom Ekman layer leading to a situation ressembling the classical "spin down" of geostrophic motions over the bottom. When the fluid is shallow, the spin up controlled by viscosity occurs more rapidly (the spin up time is then proportional to h^2/A_v).

The model values obtained after 30 days are used to analyse the differences between numerical and theoretical steady solutions. The numerical solution for the geostrophic velocity profile (figure 10a) and the stream function (figure 10b) can hardly be distinguished from the analytical solution, as they are almost identical. The largest difference occurs for the alongshore velocity (figure 10c) but remains relatively weak (< 2 cm/s). It allows us to pinpoint two sources of numerical error, namely the bottom friction parametrization and the discrete condition of no normal flow at the coast. The former comes from the no-slip condition which can only be approximated with the numerical model and affects the 3 velocity components near the bottom topography. The latter is due to the staggered grid : at the coastal boundary point a zero-gradient condition is specified for the free surface, implying a vanishing geostrophic velocity (figure 10a). This error essentially causes a lag between the numerical and theoretical alongshore flow in very shallow water.

(ii) Non linear experiment

Since the model reproduces convincingly the theory, it becomes a tool to explore the consequences of relaxing some hypotheses. In particular, we address the role of the non linear terms of the momentum equations by performing a new numerical experiment. In this case, the grid is refined near the surface and bottom boundaries and the bottom drag coefficient ($r = 7.5\ 10^{-3}$ m/s) is chosen to minimize the aforementioned error (see next paragraph on bottom friction parametrization sensitivity). The transient and stationary regimes of this experiment are close to those of the validation experiment. In particular, the near shore and deep ocean limits remain very similar. However, the non linearity has a significant influence in the transition region where upwelling occurs. The geostrophic velocity profile (figure 11a) is now smoother compared to the theory near $h/D = 0.8$. The alongshore flow

departs from the theory by about 30% at the surface in this transition region. The cross shore cell is weakened in the region of h/D between 0.5 and 1.2 while it is strengthened in deeper waters (observe the dipolar structure of the stream function difference in figure 11b). We conclude that the advection of momentum slightly amplifies the upwelling separation, by intensifying the upwelling cell around $h/D = 1.2$ and weakening it around $h/D = 0.7$. Note that the difference of vertical velocities between the linear and non linear solutions are less than a meter a day, showing that the non linear terms represent a second order correction to the linear theory given here.

(iii) Sensitivity to friction parametrizations

From a set of experiments with different values of the linear drag coefficient r, it appears that the no-slip condition can be approached by increasing r while using a refined grid in the bottom Ekman layer. Note that the primary mixing may come from tidal currents which might justify the use of a linear bottom boundary condition with a higher drag coefficient. Two other bottom friction parametrizations (quadratic and Von Karman - Prandtl type) have also been tested. An accurate control of the near bottom error is not allowed as the parametrizations are dependent on the near bottom horizontal velocity $\underline{u}_b$. For classical drag coefficient values (using $r \approx 3\ 10^{-4}$ m/s, $C_d \approx 2\ 10^{-3}$, and a roughness scale of $z_r \approx 1$ cm respectively for the linear, quadratic and logarithmic parameterizations), only the logarithmic parametrization of Von Karman - Prandtl allows to approach the no slip condition; the two other lead to an error of the same order of magnitude as the solution.

In an experiment with depth dependent turbulent viscosity profile we test Ekman's hypothesis of constant A_v. Following Prandtl's parametrization, we assume that the viscosity increases linearly from zero at the wall to a constant background value in the interior, which equals that of the validation experiment viscosity. Therefore, the associated vertical current profiles follow the logarithmic Prandtl law near the surface and bottom boundaries : $u_i = \frac{u_i^*}{\kappa} \ln \frac{z_i}{z_0}$ (where index $i = s$ or b indicates surface or bottom parametrization; reduced mixing length near the wall is $l_i = \kappa z_i$, z_i being the distance from the associated boundary and $\kappa \approx 0.4$ the Von Karman coefficient). The

applied discrete formulation is then $A_v = min\Big[A_v^{bak}, min[A_v^s, A_v^b]\Big]$, where $A_v^i = l_i^2 \frac{\partial u_i}{\partial z_i} = \kappa u_i^* z_i$ depends on the associated boundary stress through friction velocity parameter $u_i^* = \sqrt{\frac{|\tau_i|}{\rho_0}}$. In water deeper than $h/D > 0.5$, this parametrization does not affect the numerical solution which stays very close to the theoretical solution with a constant viscosity profile. In shallow water, it significantly increases the alongshore flow, but only slightly modifies the cross shore flow which remains close to zero. Consequently, upwelling occurs at about the same location and with the same magnitude (the maximum difference between the stream functions is less than 4% of the Ekman transport). This result tends to validate the constant viscosity assumption of the homogeneous fluid theory (with regards to Prandtl's parametrization). Yet, it seems at variance with the numerical experiment of Lentz (1995), who shows that upwelling properties, particularly its location, are sensitive to viscosity distributions and magnitude. Actually, inner shelf dynamics dominated by friction may be expected to produce a response to changes in viscosity when a larger range of values is considered as is the case in (Lentz 1995). Therefore, we agree with this author's conclusion that "field studies aimed at determining the characteristics of turbulence over inner shelves are clearly needed". Among other things, this would enable to make a more complete validity assessment.

The constant viscosity assumption implies the same thickness $D = \pi\sqrt{\frac{2A_v}{|f|}}$ for surface and bottom Ekman layers. This is clearly not realistic in the coastal ocean. For instance, Smith (1981) has estimated typical boundary layer thickness values in the Cap Blanc region of 30 m at the surface and 60 m at the bottom. To solve this problem analytically, one needs to consider a depth dependent viscosity (for instance a *tanh* profile with two different viscosity values between surface and bottom) and then solve equation (4) which becomes: $\partial_{zz}^2 \tilde{u}_e - \frac{\partial_z c}{c}\, \partial_z \tilde{u}_e - c^2\, \tilde{u}_e = 0$, with variable coefficient $c(z) = (1 + i\gamma)\sqrt{\frac{f}{2\,A_v(z)}}$.

(iv) On the impact of stratification

The influence of stratification is analysed using the 2D numerical model realistically configured for the wide and shallow shelf region off South Senegal (south of the Green Cape). The cross

shore bathymetric profile is extracted from GEBCO1 and the model is forced by a typical constant alongshore wind ($\tau_s^y = -0.05$ Pa). The initial stratification is at rest (horizontally uniform) and is built using temperature and salinity profiles representative of the regional climatological conditions during the upwelling season (extracted from Levitus atlas). The resulting simulation allows us to study the process of upwelling separation from the coast in a strongly stratified region. The goal here is limited to assessing the relevance of the theoretical results in a stratified context. Note that a more realistic turbulent closure [KPP (Large *et al.* 1994)] is needed to handle the influence of stratification on vertical mixing. Note also that the coupling between density and velocity fields prevents a steady state from arising and makes the comparison with the analytical steady solution more complicated.

The time evolution of density and stream function are shown in figure 12a and b for the first 10 days of integration. It takes about one day for a full Ekman transport to appear. The main difference with the homogeneous case is a cross shore oscillation of the upwelling cell (the first oscillation is completed in 6 days). The upwelling center moves between a nearshore position (30 km from the coast at days 1 and 5.5) and an offshore position (40 to 45 km at days 2.5 and 8.5). Each oscillation is made up of two phases involving different processes. First is the *outcropping* phase (between days 1 and 2.5 and between days 5.5 and 8.5) during which denser water reaches the surface and creates a density front separating a stable inner shelf front and outer shelf upwelling front. The latter is advected seaward by the surface Ekman transport leaving behind it an homogeneous water column where the surface and bottom boundary layers are fully merged (inner shelf zone); as a result, the "kinematic barrier" and upwelling cell migrates seaward with the upwelling front; the inner front stability corresponds to a thermodynamical balance between cross shore advection and vertical diffusion. Meanwhile, the uplifiting process occurring further offshore in the bottom boundary layer generates an isopycnal dome with a strongly stratified internal front. This feature is advected shoreward by the return flow; when it reaches the upwelling region, the upwelling cell ceases its seaward migration and starts moving shoreward. This is the second phase which we called *layers splitting* phase (occurring between days 2.5 and 5.5 and starting again at day 9.5). The shoreward advection of the isopycnal dome by the return flow results in full separation of surface and bottom

boundary layers. Since the boundary layers do not interact anymore the "kinematic barrier" and upwelling cell move back to shallower water, squeezing the inner shelf frictional zone against the coast. This phase yields a partial erosion of the inner front. It ends when the isopycnal dome reaches close enough to the surface to intersect the surface boundary layer; then, a new outcropping phase starts.

The nearshore end of the overturning cell is always located just offshore of the region where surface and bottom boundary layers are fully merged (i.e where both layers extends all the way through the water column). In addition, upwelling is stronger in the thin region where these layers interact (i.e where they are not fully merged neither fully separated by the stratification). These facts confirm that the mechanism for inner shelf upwelling shut down given by the theoretical model still holds in presence of strong stratification. The corresponding stream function from the steady homogeneous theory (with $D = 30$ m) is shown in figure 12c and compared with the residual numerical solution after averaging out the oscillatory contribution. It shows that the theoretical solution agrees well with the mean numerical solution, in spite of the stratification effects on the boundary layer dynamics. Some difference appears in the exact extension of upwelling divergence as a result of varying boundary layer depths in the stratified case, but the structure of the upwelling cell is preserved and has comparable dimensions. In the numerical model, the return flow seaward of the shelf break remains much longer in the ocean interior because the spin up time to build the bottom Ekman flow is proportional to depth [see section 4-(i)].

5 Concluding remarks

A two dimensional generalization of the classical 1905 Ekman's model has been developped. This theoretical model provides a rationalization for the impact of continental shelf geometry on the structure of the wind driven upwelling. In particular, the model explains the mechanism of upwelling separation from the coast which occurs in three regions of Northwest Africa. It also shows how the cross shore wind component drives the nearshore pressure gradient adjustment and how it affects

the upwelling structure. Numerical experiments have reproduced the theoretical steady solution, thereby validating the linear assumption of the theory and allowing to explore the transient regime, the sensitivity to friction parametrizations and the influence of stratification.

When applied to actual shelf topography, the analytical solution shows a satisfactory comparison with observations with the obvious caveat that the fit depends on the chosen Ekman depth. Rather than being chosen *a priori*, the turbulent viscosity coefficients need to be ultimately part of an improved theory. This would require a partitioning of the wind forcing representation, as the wind not only drives the upwelling cell but also produces the turbulence responsible for downward mixing of momentum.

Nevertheless, the present theory appears promising to characterize the geography of the wind driven upwelling structure. It provides an estimation of vertical velocity which can be used as coastal upwelling indices derived entirely from Ekman's theory (the pillar of coastal upwelling concept). It shows that 90% of the Ekman transport upwells for h/D between 1.25 and 0.5 (in the case of an alongshore wind), meaning that D/S (the ratio of Ekman depth to topographic slope) is the right scale to estimate the cross shore width of an upwelling cell. This result illustrates the frictional nature of coastal upwelling divergence. An improvement can be expected over the classical upwelling indices [derived from (Bakun 1973)], where the order of magnitude of the vertical velocity is given by the ratio of offshore Ekman transport and internal Rossby radius R'. The internal Rossby radius actually represents the cross shore scale of geostrophic adjustment of the pycnocline slope; therefore, its use in upwelling indices can be erroneous. For instance, in case of weak stratification, the Bakun index predicts a strong vertical circulation occurring in a narrow coastal band, which is certainly not the case when the continental shelf is wide and shallow. This is also predicted by the more sophisticated Pedlosky's (1978) theory which is likely more adequate for predicting upwelling over a deep and narrow shelf.

Some secondary assumptions of this two dimensional theory can be relaxed easily. For example, the cross shore variability of the Ekman depth $D(x)$ (*i.e.*, cross shore viscosity profile) and the alongshore wind stress component $\tau_s^y(x)$ can be introduced in the theory. The former case is not

useful without a cross shelf estimation of boundary layer thickness, a non trivial task by itself. By introducing wind variability, we can extend this study to the case of a cross shore wind profile and its effect on the upwelling structure. This case has been solved (not shown) for several wind profiles inducing a positive Ekman pumping effect ($\partial_x \tau_y^s > 0$). It weakens the mechanism of separation because frictional activity decreases in the nearshore region bringing the kinematic barrier and upwelling closer to the coast. Nevertheless, the upwelling cell is still mainly produced by coastal Ekman divergence rather than Ekman pumping (except in the case of a very severe nearshore wind drop off), in agreement with the numerical results of Capet et al (2004).

The theoretical model can also be used to treat wind driven downwelling problems and the "analytical upwelling" figures in this paper can be transposed to a downwelling case by sign inversion.

Among the main hypotheses, the lack of stratification and the two dimensional assumptions are the most constraining. The introduction of stratification into the numerical model (combined with a more realistic turbulence closure) modifies the upwelling structure which is no longer stationary. Yet, the mechanism of separation remains qualitatively identical. The interaction between the surface and bottom boundary layers at shallow depths still generates a kinematic barrier for the cross shore flow (although the extent to which they interact depends on the strength of the stratification). Similarly, the introduction of the alongshore dimension does not qualitatively affect the mechanism of separation but allows the development of a cross shelf geostrophic component which can strongly modify the return flow, especially in the presence of stratification. Clearly, stratified three dimensional simulations, featuring time dependent forcing and alongshore topographic variations, are needed for realistic modelling of upwelling dynamics in the outer shelf and offshore regions. However, in shallower waters the analytitical solution have much more validity with the dominance of frictional forces structured by cross shelf topography.

The theoretical solution shows that both the location of upwelling and the scale of the divergence zone (defining upwelling intensity) varies with topography. This in turn may affect frontal formation and mesoscale eddy activity (Marchesiello *et al.* 2003). The present theory provides an explanation of important differences observed in the energy of mesoscale eddies between the U.S. west coast and

Northwest African upwelling systems. Marchesiello and Estrade (2007) have conducted a comparative modelling study suggesting that stratification and topography are key parameters controlling the formation of upwelling fronts, hence the amount of energy available for mesoscale formation through baroclinic instability. The large difference in stratification appears to be linked to the salinity structure formed by the large scale circulation and is directly related to available potential energy. In addition, the shape of the continental shelf, as suggested here, affects the position, structure, and scale of the Ekman divergence, hence upwelling intensity and frontal formation. Consequently, the influence of topography on cross shelf upwelling circulation can also affect the biogeochemistry of upwelling systems through both mean and mesoscale eddy transports, explaining some of the observed differences regarding primary production (Carr 2002).

This study was motivated by observations that fish can spawn in areas that are not usually considered as favourable spawning grounds. Our theoretical approach provides a sound physical background to hypotheses based on the existence of oceanographic structures able to enhance retention over wide and shallow continental shelves. The analytical solution also provides an interpretative tool to diagnose changes in fish habitat induced by global climate change.

References

Allen, J.S., P.A. Newberger, and J. Federiuk, 1995 : Upwelling circulation on the Oregon continental shelf. Part 1 : Response to idealized forcing. *J. Phys. Oceanogr.*, **25**, 1843–1866.

Austin, J.A. and S.J. Lentz, 2002 : The inner shelf response to wind-driven upwelling and downwelling. *J. Phys. Oceanogr.*, **32**, 2171–2193.

Bakun, A., 1973 : Coastal upwelling indices, west coast of north america, 1946-71. NOAA Tech. Rep. NMFS SSRF-671, Nat. Oceanic and Atmos. Admin., Seattle, Wash.

Bakun, A., 1996 : *Patterns in the ocean. Ocean processes and marine population dynamics.* California Sea Grant College System, University of California, La Jolla, 323 pp.

Barton, E.D., A.H. Huyer, and R.L. Smith, 1977 : Temporal variation observed in the hydrographic regime near Cabo Corveiro in the Northwest African upwelling region, February to April 1974. *Deep Sea Res.*, **24**, 7–23.

Brink, K.H., 1983a : Low-frequency free wave and wind-driven motions over a submarine bank. *J. Phys. Oceanogr.*, **13**, 103–116.

Brink, K.H., 1983b : The near-surface dynamics of coastal upwelling. *Prog. Oceanog.*, **12**, 223–257.

Capet, X., P. Marchesiello, and J.C. McWilliams, 2004 : Upwelling response to coastal wind profiles. *Geophys. Res. Lett.*, **13**, L13311, doi: 10.1029/2004GL020123.

Carr, M.E., 2002 : Estimation of potential productivity in eastern boundary currents using remote sensing. *Deep Sea Res.*, **49**, 59–80.

Csanady, G.T., 1982 : *Circulation in the Coastal Ocean.* D. Reidel Publising Company.

Demarcq, H. and V. Faure, 2000 : Coastal upwelling and associated retention indices derived from satellite SST. Application to Octopus vulgaris recruitment. *Oceanolo. Acta*, **23**, 391–407.

Ekman, V.W., 1905 : On the influence of the earth's rotation on ocean-currents. *Arkiv. Mat. Astron. Fysik*, **2**, 1–53.

Garrett, C., P. McCready, and P. Rhines, 1993 : Boundary mixing and arrested Ekman layers : rotating stratified flow near a sloping boundary. *Annu. Rev. Fluid. Mech.*, **25**, 291–323.

Greenspan, H.P., 1968 : *The theory of rotating fluids*. Cambridge Univ. Press.

Hill, A.E., B.M. Hickey, F.A. Shillington, P.T. Strub, K.H. Brink, E.D. Barton, and A.C. Thomas, 1998 : Eastern ocean boundaries coastal segment (e). *The Sea*, **11**, 29–67.

Hill, R.B. and J.A. Johnson, 1974 : A theory of upwelling over the shelf break. *J. Phys. Oceanogr.*, **4**, 19–26.

Hsueh, Y. and H.W. Ou, 1975 : On the possibilities of coastal, mid-shelf, and shelf break upwelling. *J. Phys. Oceanogr.*, **5**, 670–682.

Huyer, A., 1976 : A comparison of upwelling events in two locations : Oregon and Northwest Africa. *J. Mar. Res.*, **34**, 531–546.

Johnson, J.A. and P.D. Killworth, 1975 : A bottom current along the shelf break. *J. Phys. Oceanogr.*, **5**, 185–188.

Johnson, J.A. and B.A. Manja, 1979 : Shear layers above a break in bottom topography. *Geophys. Astrophys. Fluid Dynamics*, **14**, 45–60.

Johnson, J.A. and A.J.G. Nurser, 1983 : A model of secondary upwelling over the shelf break. *Geophys. Astrophys. Fluid Dynamics*, **23**, 301–320.

Kirincich, A.R., J.A. Barth, B.A. Grantham, B.A. Menge, and J. Lubchenco, 2005 : Wind-driven inner-shelf circulation off central Oregon during summer. *J. Geophys. Res.*, **110**, doi:10.1029/2004JC002611.

Kundu, P.K., 1977. On the importance of friction in two typical continental waters : off Oregon and Spanish Sahara. In J. Nihoul (Ed.), *Bottom turbulence*, pp. 187–207. 8th Lige Colloq. Ocean Hydrodyn. (1976).

Large, W.G., J.C. McWilliams, and S.C. Doney, 1994 : Ocean vertical mixing : a review and a model with a nonlocal boundary layer parametrization. *Rev. Geophys.*, **32**, 363–403.

Lentz, S.J., 1992 : The surface boundary layer in coastal upwelling regions. *J. Phys. Oceanogr.*, **22**, 1517–1539.

Lentz, S.J., 1995 : Sensitivity of the inner-shelf circulation to the form of the eddy viscosity profile. *J. Phys. Oceanogr.*, **25**, 19–28.

Lentz, S.J. and D.C. Chapman, 2004 : The importance of nonlinear cross-shelf momentum flux during wind-driven coastal upwelling. *J. Phys. Oceanogr.*, **34**, 2444–2457.

Lill, C.C., 1979 : Upwelling over the shelf break. *J. Phys. Oceanogr.*, **9**, 1044–1047.

Marchesiello, P. and P. Estrade, 2007 : Eddy activity and mixing in upwelling systems : A comparative study of Northwest Africa and California regions. *International Journal of Earth Sciences*, DOI 10.1007/s00531–007–0235–6.

Marchesiello, P., M.T. Gibbs, and J.H. Middleton, 2000 : Simulations of coastal upwelling on the Sydney continental shelf. *Mar. Freshwater Res.*, **51**, 577–588.

Marchesiello, P., J.C. McWilliams, and A. Shchepetkin, 2003 : Equilibrium structure and dynamics of the California Current System. *J. Phys. Oceanogr.*, **33**, 753–783.

Mitchum, G.T. and A.J. Clarke, 1986 : The frictional nearshore response to forcing by synoptic scale winds. *J. Phys. Oceanogr.*, **16**, 934–946.

Mittelstaedt, E., 1983 : The upwelling area off Northwest Africa - A description of phenomena related to coastal upwelling. *Prog. Oceanog.*, **12**, 307–331.

Parrish, R.H., A. Bakun, D.M. Husby, and C.S. Nelson, 1983 : Comparative climatology of selected environmental processes in relation to eastern boundary current pelagic fish reproduction. In J. C. G.D. Sharp (Ed.), *Proceedings of the expert consultation to examine changes in abundance and species composition of neritic fish resources*, Volume 291, pp. 731–778.

Pedlosky, J., 1978 : An inertial model of steady coastal upwelling. *J. Phys. Oceanogr.*, **8**, 171–177.

Pedlosky, J., 1987 : *Geophysical Fluid Dynamics*. Springer-Verlag.

Pickett, M.H. and J.D. Paduan, 2003 : Ekman transport and pumping in the California current based on the US Navy's high resolution atmospheric model (COAMPS). *J. Geophys. Res.*, **108 (C10)**, doi:10.1029/2003JC001902.

Pond, S. and G.L. Pickard, 1986 : *Introductory dynamical oceanography*. Pergamon Press, 329 pp.

Roy, C., 1998 : An upwelling-induced retention area off Senegal : a mechanism to link upwelling and retention processes. *S. Afr. J. Mar. Sci.*, **19**, 89–98.

Roy, C., P. Cury, A. Fontana, and H. Belvze, 1989 : Stratégies spatio-temporelles de la reproduction des clupéidés des zones d'upwelling d'Afrique de l'Ouest. *Aquat. Living Resour.*, **2**, 21–29.

Scor Working Group, 1975 : Coastal upwelling processes. *CUEA Newsletter 4*(3), 12–20.

Shchepetkin, A.F. and J.C. McWilliams, 2005 : The regional oceanic modeling system (ROMS) : a split-explicit, free-surface, topography-following-coordinate oceanic model. *Ocean Modelling*, **9**, 347–404.

Smith, R.L., 1981. A comparison of the structure and variability of the flow field in three coastal upwelling regions : Oregon, Northwest Africa, and Peru. In F. Richards (Ed.), *Coastal upwelling*, pp. 107–118. Amer. Geophys. Union.

Tennekes, H. and J.L. Lumley, 1987 : *A first course in turbulence*. The MIT Press.

Tomczak, M. and R.H. Käse, 1974 : A linear theory of stationary coastal upwelling in a continuously stratified ocean with an unstratified shelf area. *J. Mar. Res.*, **32**, 365–376.

Welander, P., 1957 : Wind action in a shallow sea : some generalizations of Ekman's theory. *Tellus*, **9**, 45–52.

Wooster, W.S., A. Bakun, and D.R. McLain, 1976 : The seasonal upwelling cycle along the eastern boundary of the North Atlantic. *J. Mar. Res.*, **34**, 131–141.

List of Figures

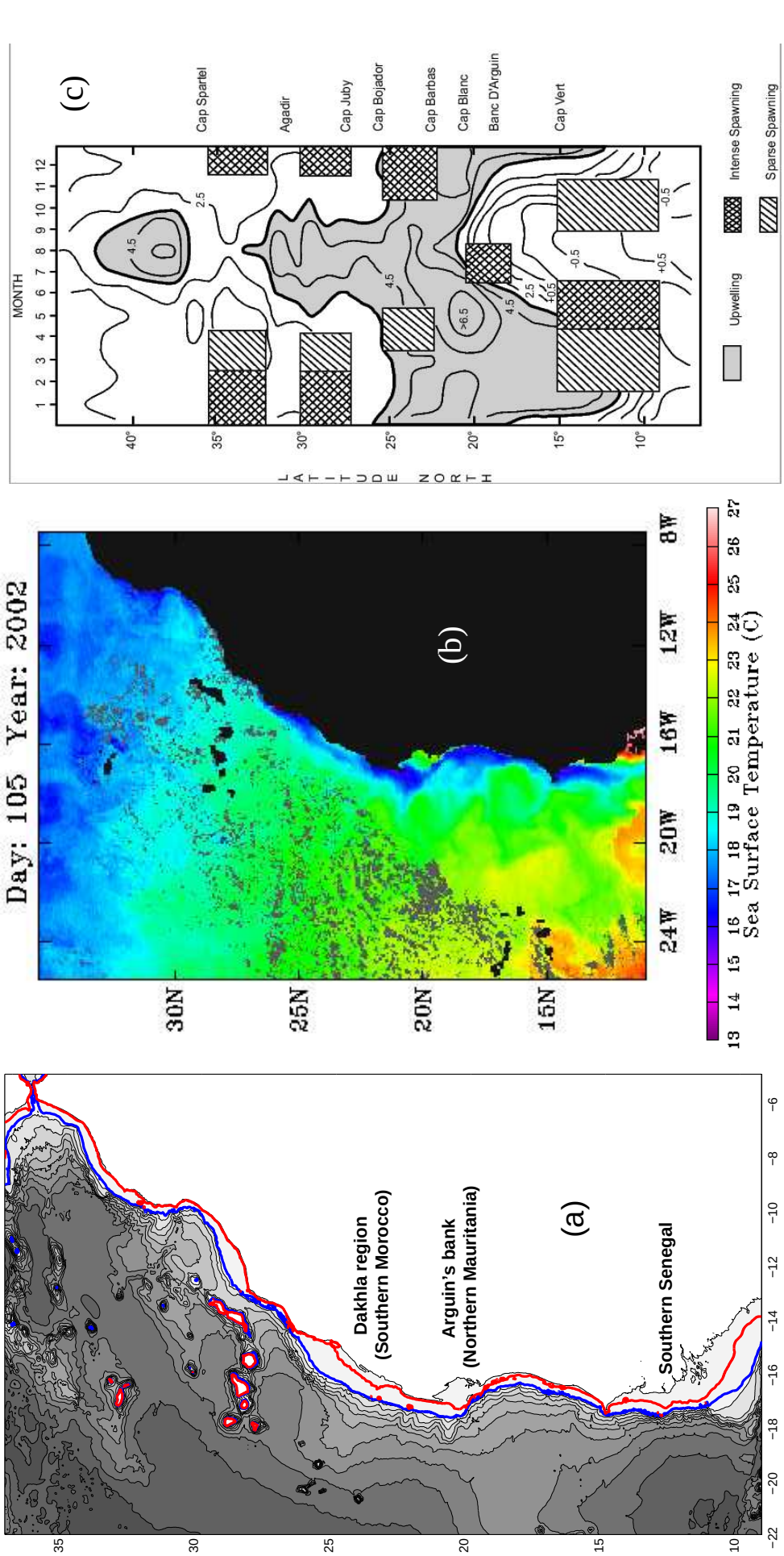

(c) Spatial and temporal distribution of clupeids spawning (Roy *et al.* 1989), superposed on an upwelling index showing difference between offshore and coastal sea surface temperatures (Wooster *et al.* 1976). The gray shaded area demarks index values greater than 3.5^oC.

(b) 7-day Composite of MODIS SST images at 4 km resolution for the second week of April 2004 (from PO.DAAC).

(a) Bathymetry from Gebco1 (resolution 1'). Black contours represent isobaths from 0 to 6000 m (with 500 m contour interval). Blue and red contours represent respectively isobaths 200 m and 30 m.

Figure 1: Topography, upwelling structure and fish reproduction strategies off Northwest Africa.

$$
\begin{aligned}
\alpha = &\quad [\cosh(\eta)\cos(\eta)]^2 + [\sinh(\eta)\sin(\gamma\eta)]^2 \\
S_1 = &\quad \cosh(\eta)\cos(\eta)\,\alpha^{-1}(\eta) \\
S_2 = &\quad \sinh(\eta)\sin(\gamma\eta)\,\alpha^{-1}(\eta) \\
T_1 = &\quad \cosh(\eta)\sinh(\eta)\,\alpha^{-1}(\eta) \\
T_2 = &\quad \cos(\eta)\sin(\gamma\eta)\,\alpha^{-1}(\eta) \\
F_1 = &\quad \sinh(\eta)\cos(\eta) \\
F_2 = &\quad \cosh(\eta)\sin(\gamma\eta)
\end{aligned}
$$

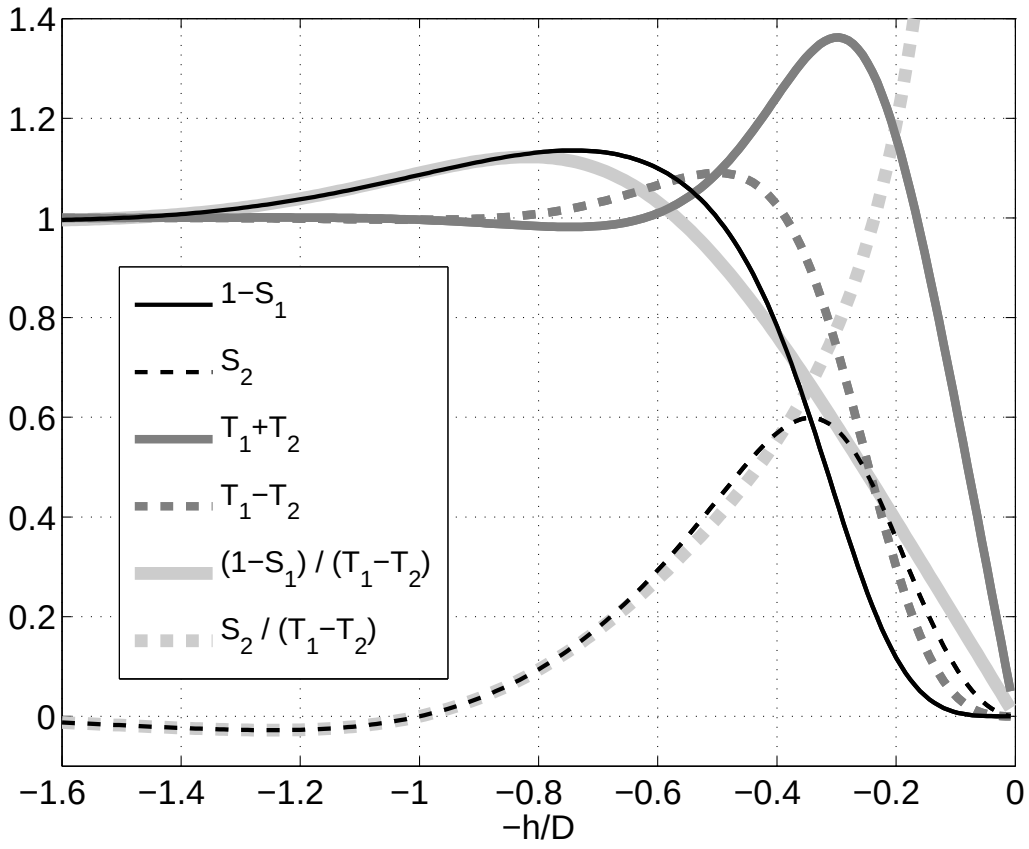

Figure 2: Structure functions of $\eta = \frac{\pi h}{D}$ in northern hemisphere ($\gamma = 1$). They have useful properties: $\cosh[ch] = \alpha(S_1 + i\,S_2)$, $\cosh^{-1}[ch] = S_1 - i\,S_2$, $\sinh[ch] = F_1 + i\,F_2$, $(F_1 + i\,F_2)(S_1 - i\,S_2) = T_1 + i\,T_2$, $\alpha({S_1}^2 + {S_2}^2) = 1$. For asymptotic considerations, it is interesting to note that deep ocean limit is 0 for S_1, S_2, T_2 and 1 for T_1 (roughly for $h/D > 1.5$).

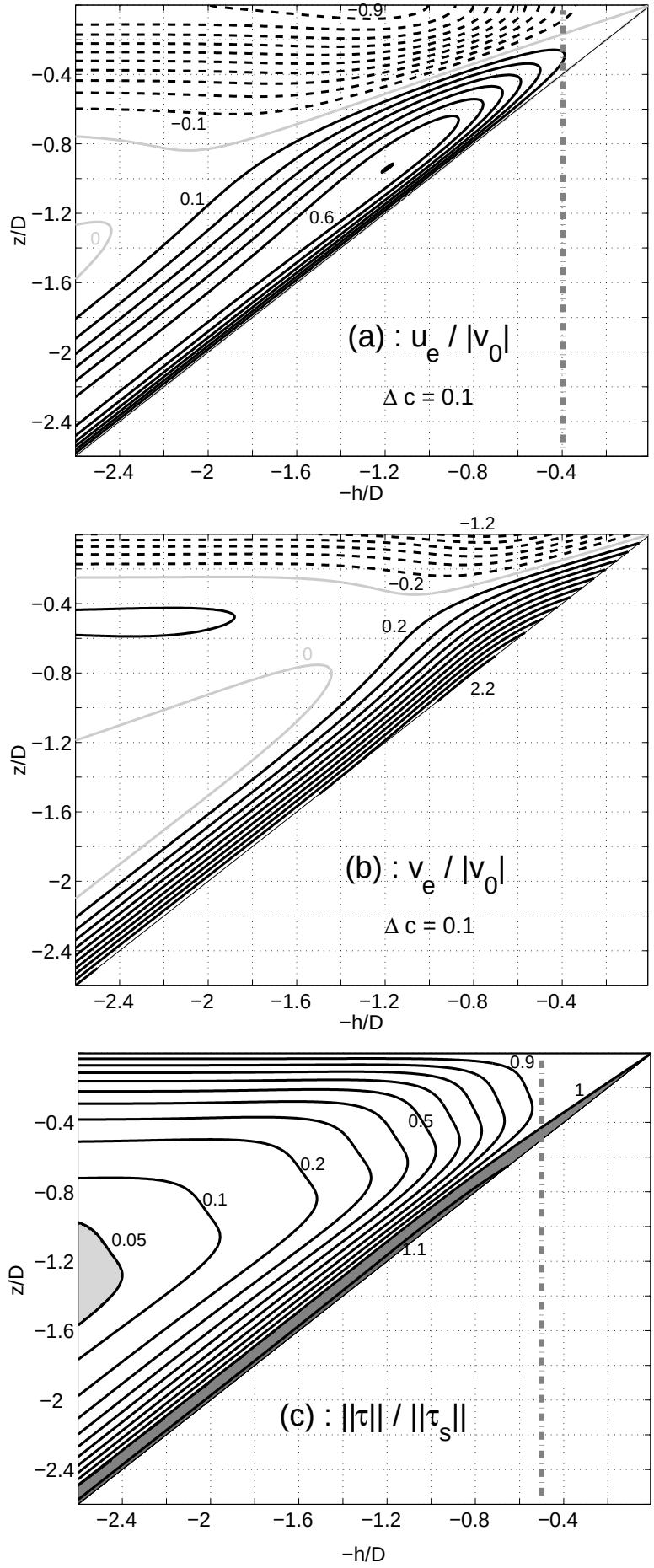

Figure 3: (a) & (b) Normalized structure of horizontal components of the Ekman flow (Δc is the contour interval). (c) Stress normalized by surface wind stress.

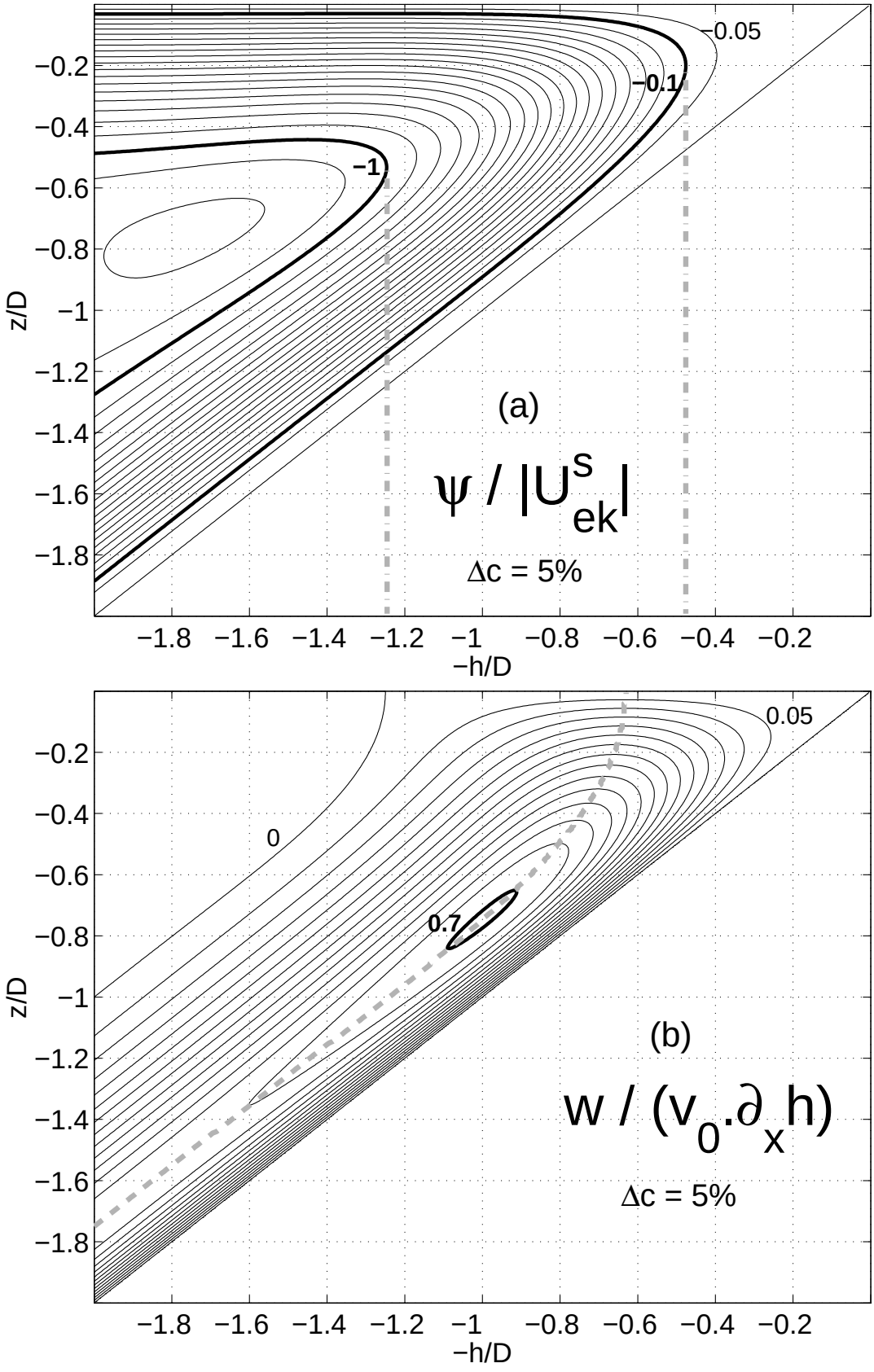

Figure 4: (a) Stream function normalized by Ekman transport $|\frac{\tau_s^y}{\rho_0 f}|$. (b) Vertical velocity normalized by wind forcing and slope topography (the dash gray contour indicates maximum for each vertical coordinate z, therefore it represents the preferential way for upwelling). Contour interval is 5% for these 2 figures.

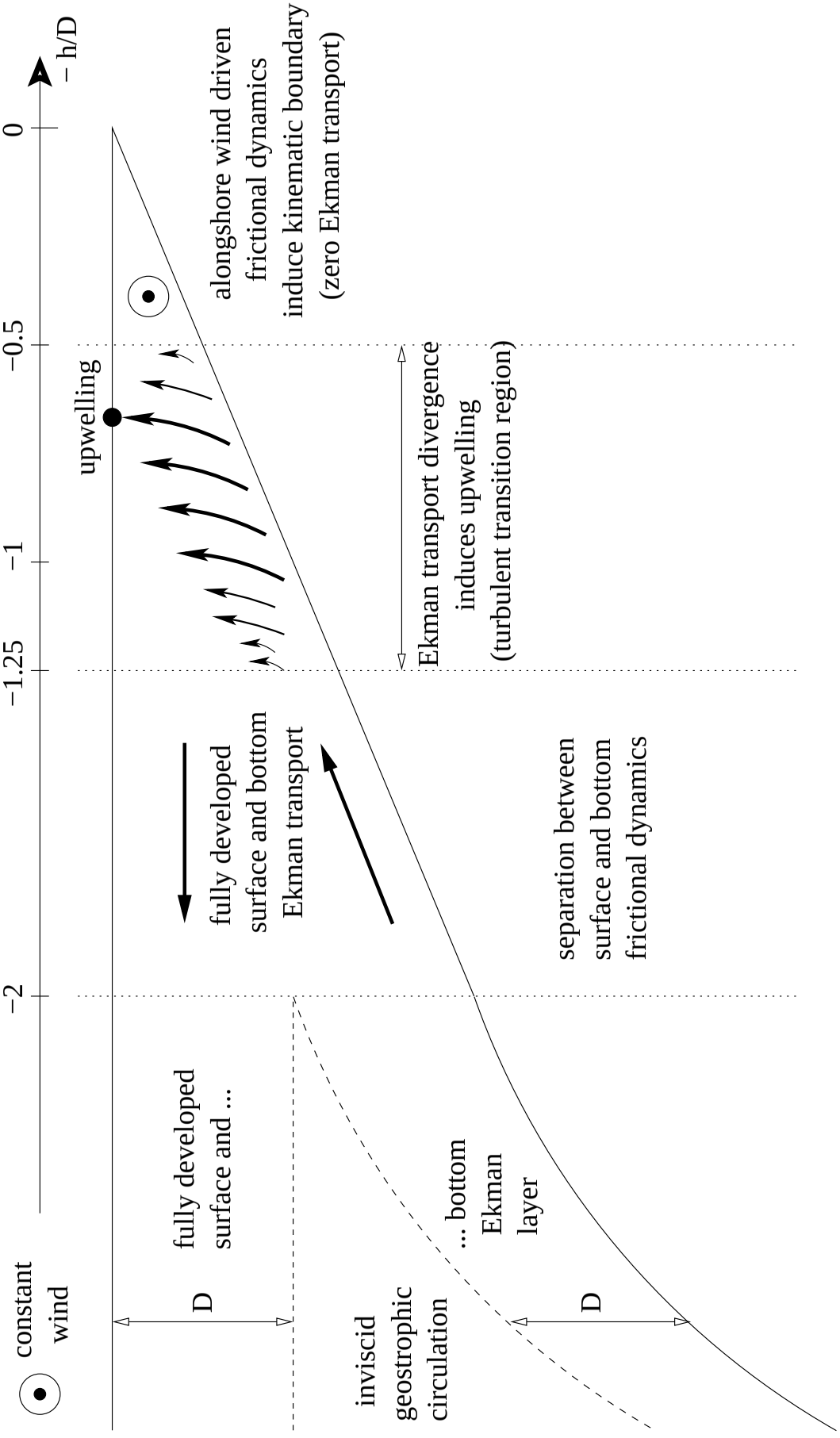

Figure 5: Conceptual scheme of the mechanism of upwelling separation from the coast

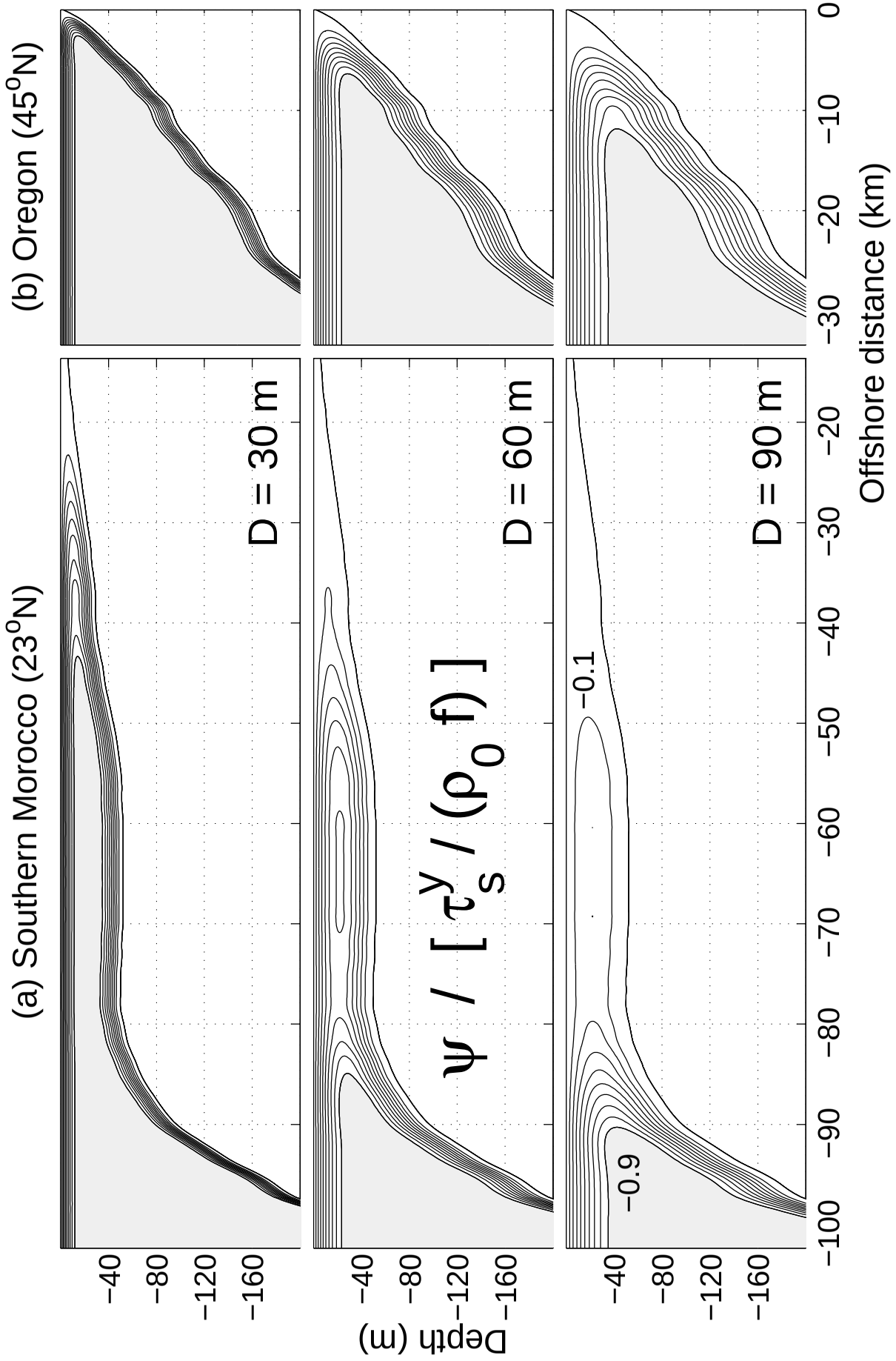

Figure 6: Normalized stream function applied to typical topographic profiles off Southern Morocco (a) and Oregon (b). Contours are shown from -0.9 to 0 with interval of 0.1.

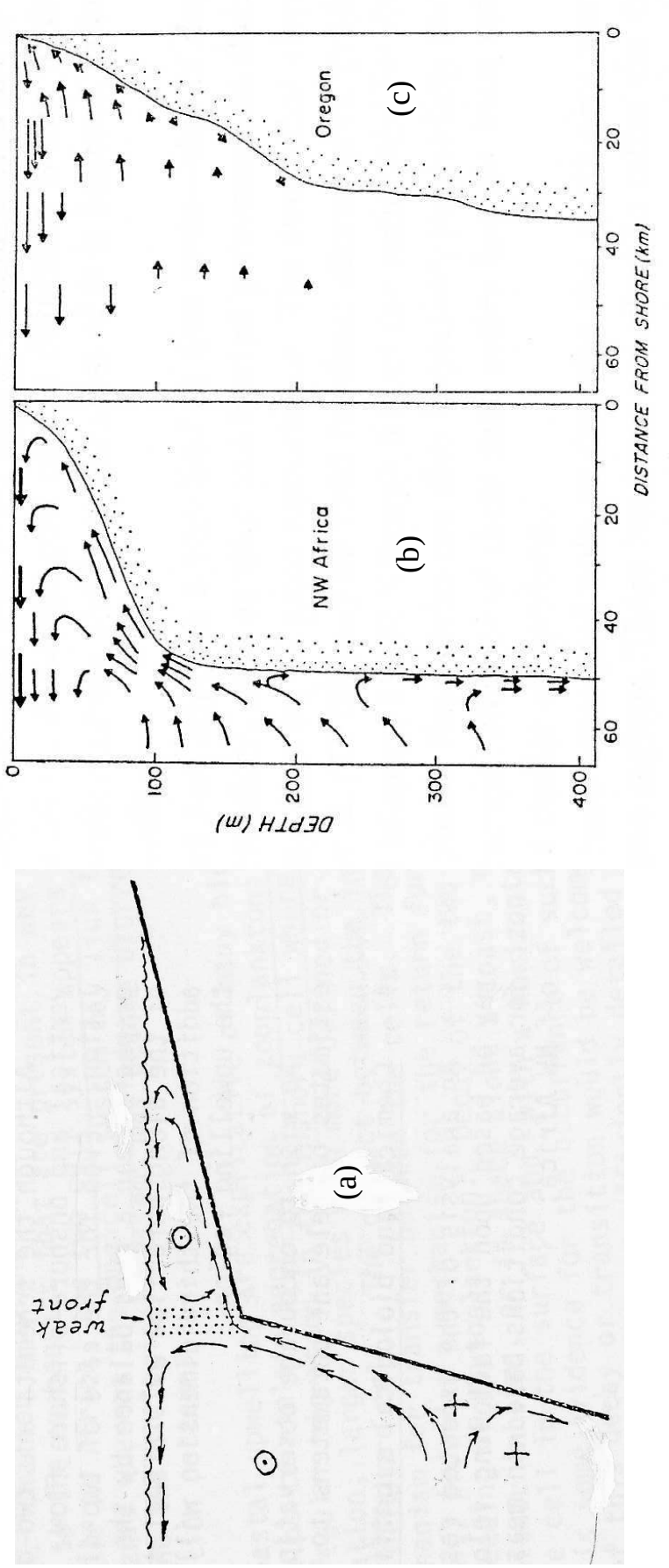

Figure 7: Upwelling cell schemes based on observations. (a) Southern Morocco (Scor Working Group 1975). (b) Region of Cape Blanc (Mittelstaedt 1983). (c) Oregon (Huyer 1976). (b) and (c) are extracted from (Huyer 1976).

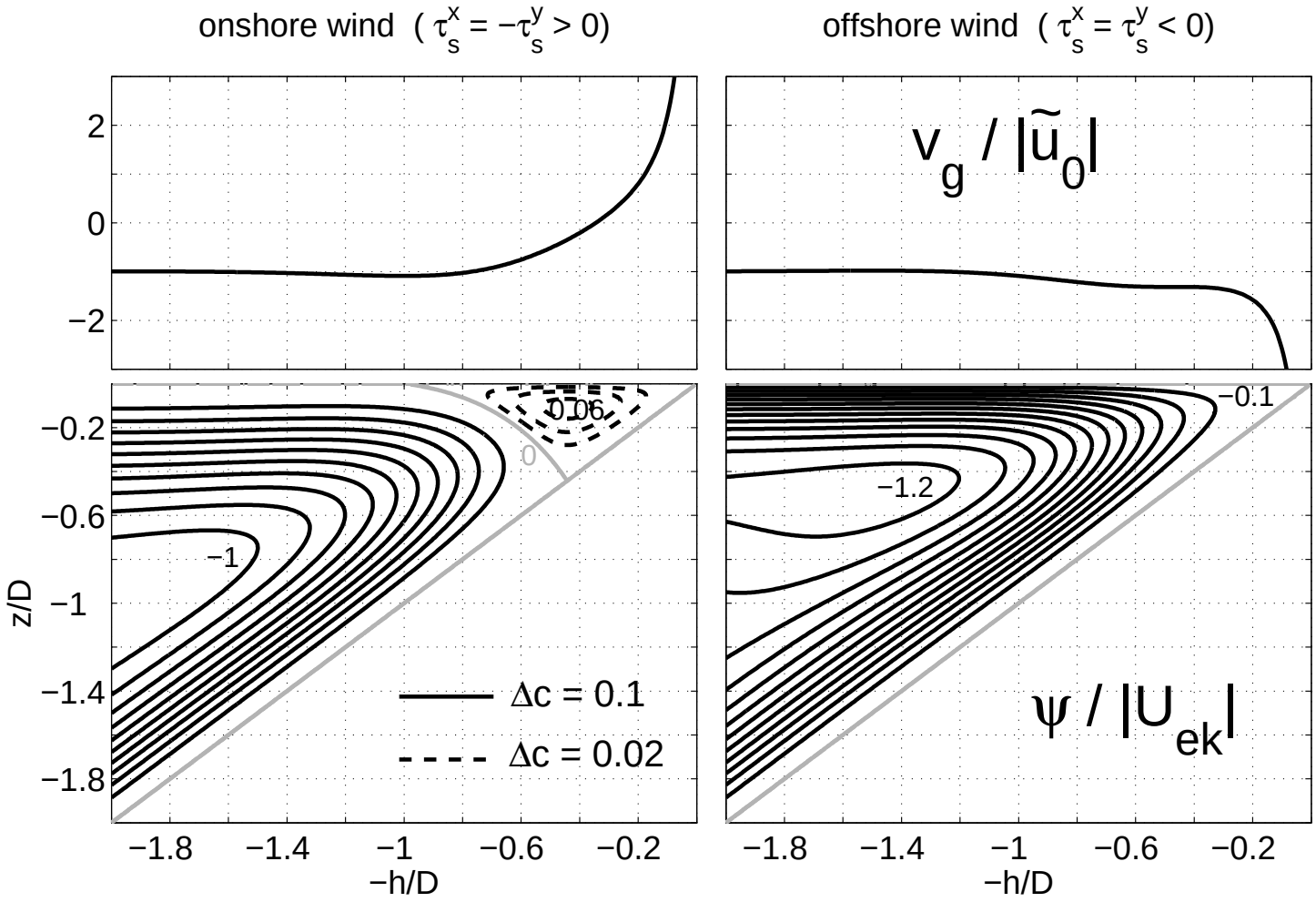

Figure 8: Upwelling effect of the cross shore component of the wind. Top : Normalized geostrophic velocity. Bottom : Normalized stream function.

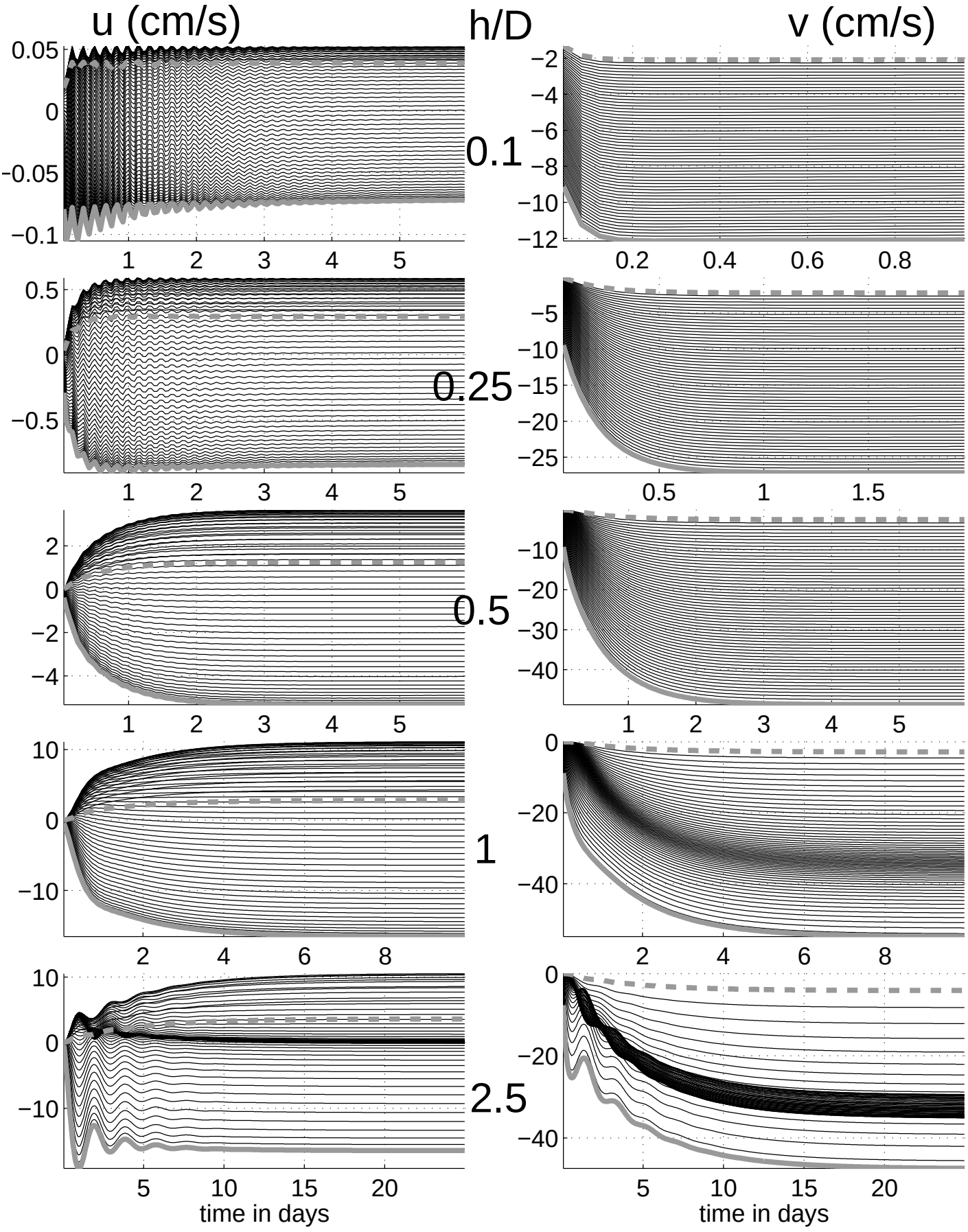

Figure 9: Transient state of the validation experiment. Time evolution of horizontal velocities, at different cross shore positions given by h/D values, are plotted for each vertical level. The nearest level from free surface [bottom topography] is plotted in solid [dash] gray.

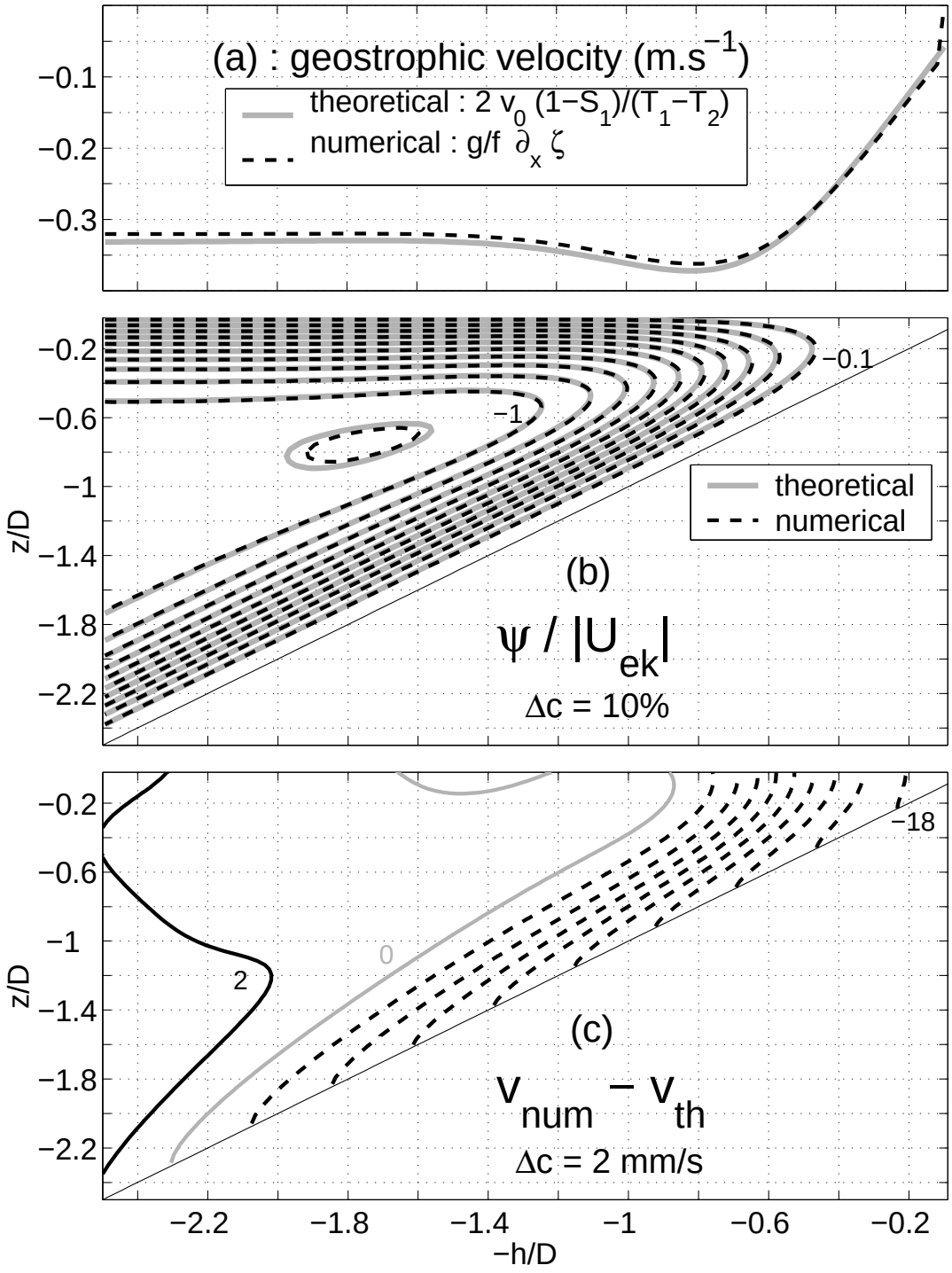

Figure 10: Comparison of steady state validation experiment results (at day 30) with theoretical solution. (a) geostrophic velocity profiles. (b) : normalized stream functions. (c) : numerical error on alongshore velocity compared with the theory.

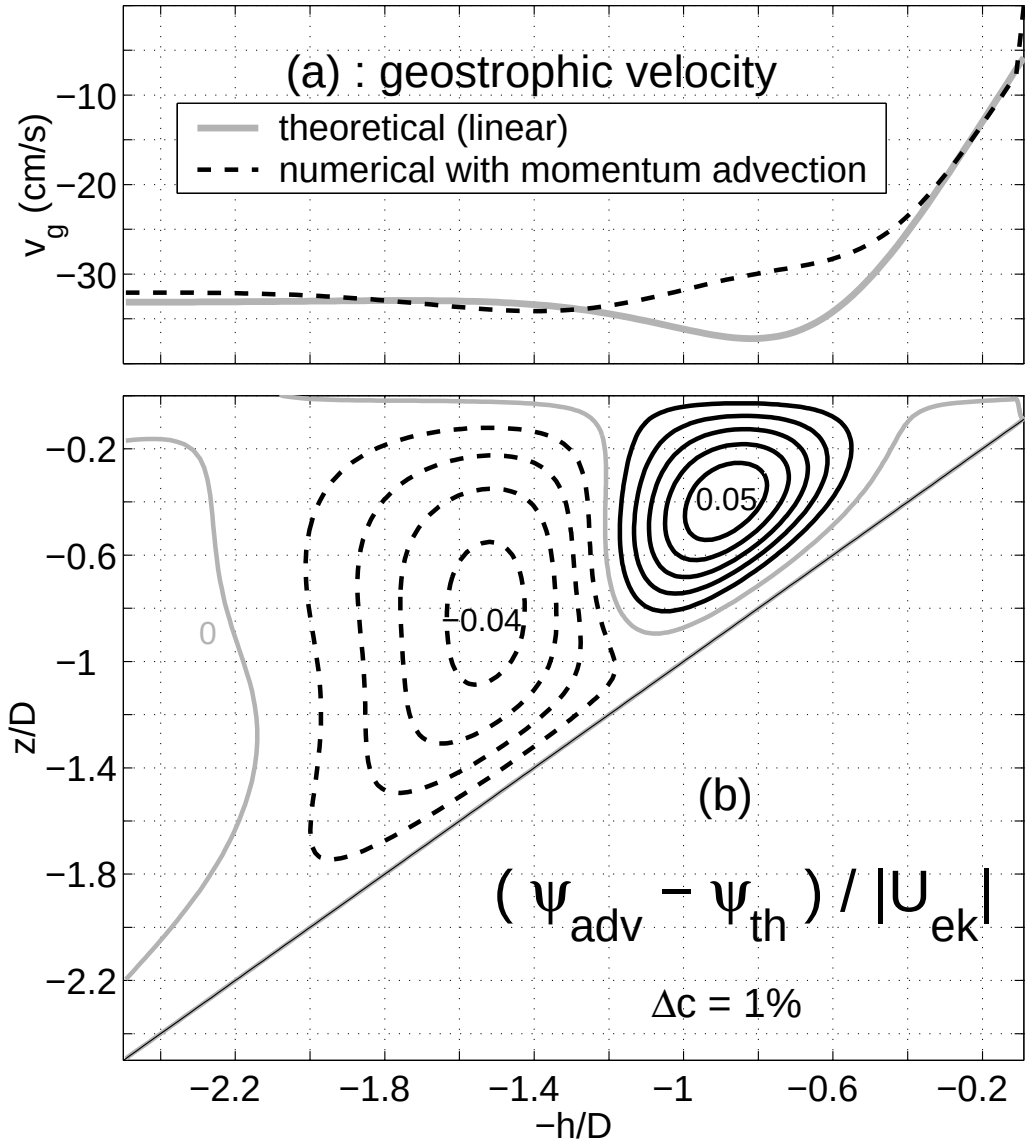

Figure 11: Comparison of non linear experiment results at steady state (day 30) with linear theoretical solution. (a) pressure gradient. (b) stream function normalized by Ekman transport.

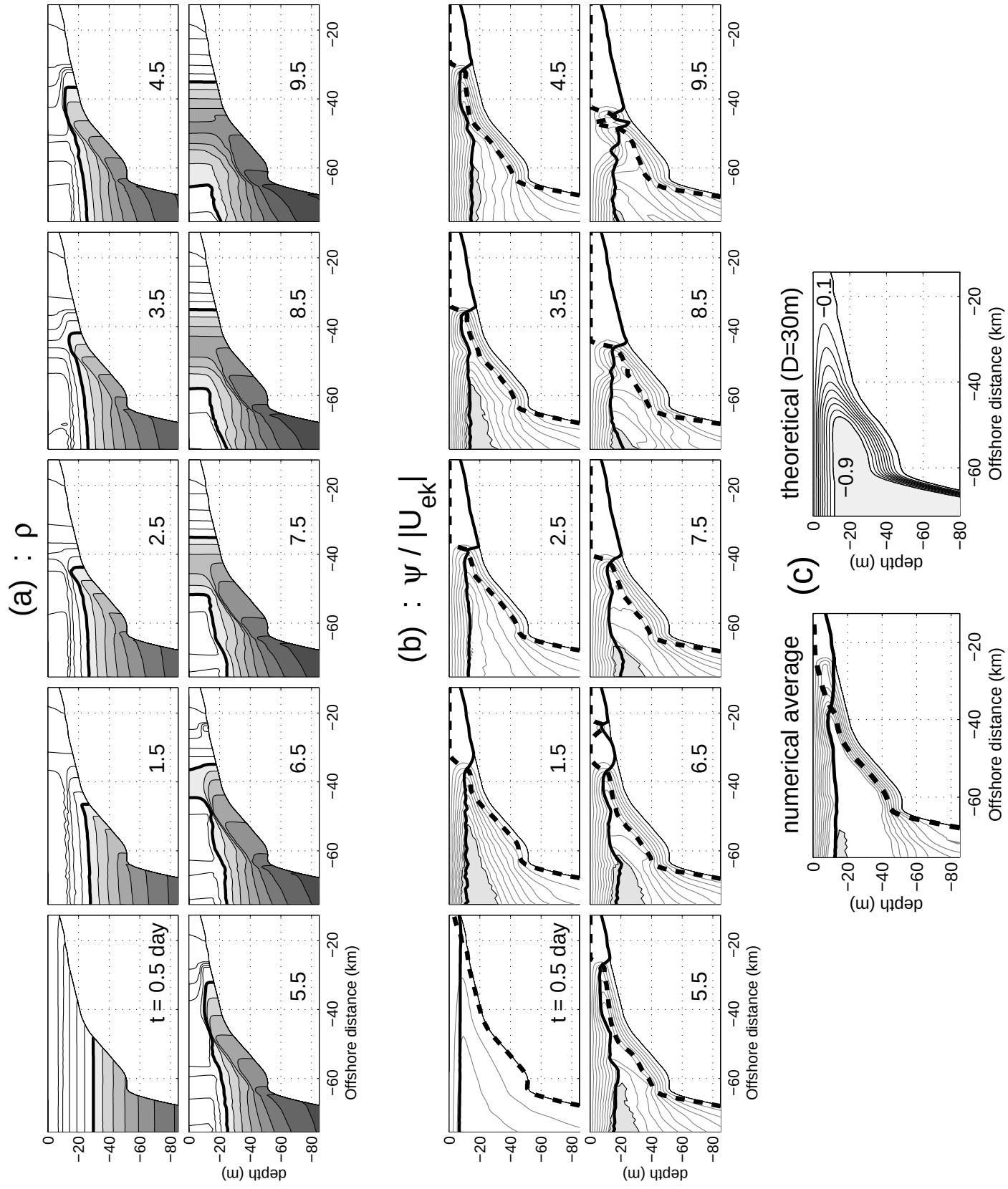

Figure 12: Stratification effect on the upwelling cell in the Senegal numerical experiment (results are zoomed around the upwelling region). (a) : Density (contour interval is 0.2 $kg.m^{-3}$). (b) : Normalized stream function [same contours as in (c)] superposed with the surface and bottom boundary layer depths given by KPP [respectively solid and dash thick contour]. (c) : comparison between the numerical solution averaged over the first oscillation (between days 0 and 6) and the analytical (homogeneous and steady) solution for $D = 30$ m.